Journal of Materials Chemistry B

PAPER

View Article Online
View Journal | View Issue

Check for updates

Cite this: J. Mater. Chem. B, 2023, 11, 3951

A mitochondria-targeting self-assembled carrier-free lonidamine nanodrug for redox-activated drug release to enhance cancer chemotherapy†

Ting Yang,‡[ab] Xianfen Zhang,‡[ac] Xing Yang,[a] Ying Li,[a] Jingjing Xiang,[a] Chunbai Xiang,[a] Zhongke Liu,[ad] Luo Hai,[e] Saipeng Huang, *[c] Lihua Zhou, *[f] Ruijing Liang *[a] and Ping Gong*[a]

Received 15th December 2022,
Accepted 21st March 2023

DOI: 10.1039/d2tb02728c

rsc.li/materials-b

Mitochondria play a vital role in maintaining cellular homeostasis. In recent years, studies have found that mitochondria have an important role in the occurrence and development of tumors, and targeting mitochondria has become a new strategy for tumor treatment. Lonidamine (LND), as a hexokinase inhibitor, can block the energy supply and destroy mitochondria. However, poor water solubility and low mitochondrial selectivity limit its clinical application. To overcome these obstacles, we report redox-activated self-assembled carrier-free nanoparticles (Cy-TK-LND NPs) based on a small molecule prodrug, in which photosensitizer IR780 (Cy) which targets mitochondria is conjugated to LND *via* a sensitive thioketal (TK) linker. Intracellular oxidative stress induced by laser radiation leads to the responsive cleavage of Cy-TK-LND NPs, facilitating the release of free LND into mitochondria. Subsequently, LND damages mitochondria, triggering the apoptosis pathway. The results show the effective killing effect of Cy-TK-LND NPs on cancer cells *in vitro* and *in vivo*. The IC_{50} value of irradiated Cy-TK-LND NPs is 5-fold lower than that of free LND. Moreover, tumor tissue section staining results demonstrate that irradiated Cy-TK-LND NPs induce necrosis and apoptosis of tumor cells, upregulate cytochrome *C* and pro-apoptotic Bax, and downregulate anti-apoptotic Bcl-2. Generally, Cy-TK-LND NPs exhibit efficient mitochondria-targeted delivery to improve the medicinal availability of LND. Accordingly, such a carrier-free prodrug-based nanomedicine holds promise as an effective cancer chemotherapy strategy.

Introduction

A major public human health problem that mankind has to solve is improving the efficacy of cancer therapy.[1] Recently, novel cancer treatment strategies have emerged, but chemotherapy is still commonly applied in clinics for various cancers.[2,3] However, the poor physicochemical properties and insufficient targeting ability of chemotherapy drugs clinically lead to serious systemic toxicity to normal tissues, challenging achieving the ideal therapeutic effects.[4] Nowadays, nanomedicine shows great potential in tumor prevention, early diagnosis, and treatment.[5,6] The unique advantages of nanomedicine over traditional chemotherapy drugs include (1) improving drug solubility and dispersion, and prolonging the circulation time in the blood; (2) increasing the accumulation and penetration of drugs at disease sites, reducing the severe side-effects; and (3) enhancing efficacy through co-delivering with multiple therapeutic agents for synergistic therapy.[7–9] Nevertheless, most nanomedicine developments into approved treatment modalities remain constrained. One reason is that the introduction of a large number of carrier materials makes the preparation of nanoparticles difficult, which is not conducive to commercial mass production. Besides, the extremely

[a] Guangdong Key Laboratory of Nanomedicine, CAS-HK Joint Lab for Biomaterials, Shenzhen Institutes of Advanced Technology, Chinese Academy of Sciences, Shenzhen, 518055, P. R. China. E-mail: rj.liang@siat.ac.cn, ping.gong@siat.ac.cn
[b] University of Chinese Academy of Sciences, Beijing, 100049, P. R. China
[c] School of Chemical Engineering, Northwest University, Xi'an, 710069, P. R. China. E-mail: huangsaipeng@nwu.edu.cn
[d] Nano Science and Technology Institute, University of Science & Technology of China, Suzhou, 215123, P. R. China
[e] Central Laboratory, National Cancer Center/National Clinical Research Center for Cancer/Cancer Hospital & Shenzhen Hospital, Chinese Academy of Medical Sciences and Peking Union Medical College, Shenzhen, 518116, P. R. China
[f] School of Applied Biology, Shenzhen Institute of Technology, No. 1 Jiangjunmao, Shenzhen, 518116, P. R. China. E-mail: zhoulihuasit@163.com

† Electronic supplementary information (ESI) available. See DOI: https://doi.org/10.1039/d2tb02728c

‡ These authors contributed equally to this work.

complicated fabrication process also causes uncontrolled drug release in circulation and low accumulation at focal sites.[10–12]

Recent cancer therapy research has gradually focused on the self-assembled carrier-free nanoparticle drug delivery systems (nano-DDSs) based on small molecule prodrugs, a simple and efficient strategy. Through the rational design of the linker, these nano-DDSs can respond to endogenous stimuli (*e.g.*, pH, enzyme, GSH, *etc.*)[13–16] or exogenous stimuli (*e.g.*, light, ultrasound, *etc.*)[17–19] to release drugs on-demand. More importantly, the abnormal metabolism of cancer cells causes increased oxidative stress, with a 1,000-fold higher ROS level within the cancer cells as compared to the normal cells.[20] Meanwhile, cancer cells also produce a high level of prototype GSH (10 mM) to maintain a dynamic redox balance.[21,22] Therefore, an oxidation- and reduction-responsive nano-DDS was widely used.[23–25] Moreover, a carrier-free nano-DDS composed of several active agents without additional exogenous excipients possesses high drug loading and low toxicity.[26,27] Zhang *et al.* designed a pure DOX nanoparticle, the drug payload of which reached as high as 90.47%.[28] However, these nanodrugs are formed by binding therapeutic agents only and lack targeting ligands, which results in insufficient targeted delivery efficiency. Some studies reported that certain heptamethine carbocyanine dyes can be transported inside the cells through organic anion transporters (OATPs), especially OATP1B3, that are highly expressed on the surface of cancer cells.[29–31] Using this "structural inherent targeting" strategy, Shi *et al.* synthesized a series of NIR fluorescent molecules.[32,33] This strategy needs to be considered in the design of nanomedicine to achieve precision in cancer treatment, especially for those therapeutic drugs which act in specific subcellular structures.

Mitochondria are the most critical subcellular organelle that plays a vital role in providing energy to the cells and regulating the cell apoptosis pathway.[34,35] Tumor cells are more easily affected by mitochondrial disorders than normal cells,[36] making mitochondria an appealing alternate target to achieve precision chemotherapeutic drug delivery for cancer therapy. Several targeted moieties (*e.g.*, triphenylphosphonium (TPP) and cationic peptides) have excellent mitochondrial accumulation ability, which coincides with the characteristics of hyperpolarized membrane potential (ΔΨm) and lipophilicity of mitochondria.[37–39] Lonidamine (LND), a broad-spectrum antitumor drug, can selectively restrict aerobic glycolysis and energy metabolism in tumor cells by inhibiting the hexokinase activity of the mitochondria.[40] Besides, LND can also directly disrupt the mitochondrial transmembrane potential to activate the downstream caspase cascade pathway that eventually leads to apoptosis.[41,42] Nevertheless, the disadvantages of poor water solubility and lack of mitochondrial selectivity limit the application of LND in clinical oncology treatment.[43]

In light of the above considerations, we designed a redox-activated self-assembled carrier-free nanoparticle (denoted as Cy-TK-LND NPs) based on a small molecule prodrug, with mitochondria-targeted and temporal and spatial drug release properties for cancer precision therapy (Fig. 1). The prodrug was composed of a photosensitizer IR780 (Cy), which targets

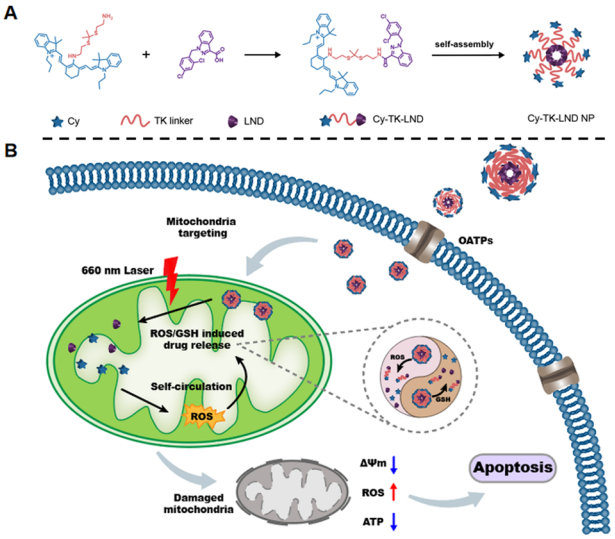

Fig. 1 (A) Schematic illustration of the chemical structure of prodrug Cy-TK-LND. (B) Schematic illustration of Cy-TK-LND NPs targeting mitochondria and activation of the mitochondrial apoptosis pathway.

mitochondria, and LND linked by a sensitive thioketal (TK) linker, and self-assembled to generate Cy-TK-LND nanodrugs in an aqueous environment. The Cy-TK-LND NPs targeted the cancer cells through the OATP mediated transport, and could be accurately delivered to the mitochondria. Subsequently, intracellular oxidative stress induced by laser irradiation disrupted the original dynamic equilibrium, increasing the levels of ROS and GSH, which in turn promoted the cleavage of the TK linker in the prodrug. The mitochondrial apoptosis pathway was then activated by the released LND, significantly enhancing the anticancer effect. The composition of this nano-DDS is extremely simple, due to the structure of IR780 possessing inherent targeting capabilities for tumor cells and mitochondria. With no extra carriers being introduced, the prodrug molecules were both cargoes and carriers of nanoparticles, enhancing the load of the chemotherapeutic drug. Generally, the obtained Cy-TK-LND NPs exhibited low toxicity, efficient delivery rates, and biodegradability improving the medicinal availability of LND. Such an engineered mitochondria-targeting nano-DDS based on a prodrug is a potent strategy to improve the clinical availability of chemotherapeutic drugs.

Results and discussion

The Cy-TK-LND prodrug molecules were synthesized through coupling TK-modified Cy and activated LND molecules. The synthetic pathway is shown in Fig. S1 (ESI†). ^{1}H NMR and ^{13}C NMR spectra, and high-resolution mass spectroscopy (HRMS), were used to describe the chemical structures of related synthetic products, revealing that the prodrug Cy-TK-LND was successfully constructed (Fig. S2–S4, ESI†). Dynamic light scattering (DLS) analysis revealed that the average diameter of Cy-TK-LND NPs was around 150 nm, and the uniform spherical morphology was validated by transmission electron microscopy

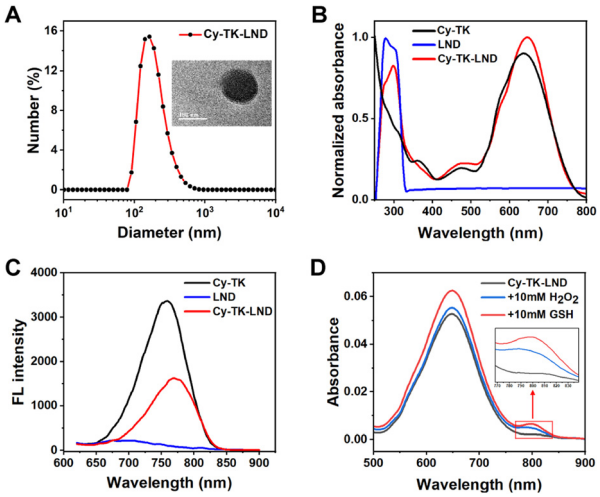

Fig. 2 Physiochemical characterization studies of Cy-TK-LND NPs. (A) Size distribution and TEM image of Cy-TK-LND NPs. (B) UV-vis absorption of Cy-TK, LND, and Cy-TK-LND NPs. (C) Fluorescence emission spectra of Cy-TK, LND, and Cy-TK-LND NPs (λ_{ex} = 650 nm). (D) UV-vis absorption changes of Cy-TK-LND NPs in 10 mM H_2O_2 solution (with 3.2 μM $CuCl_2$) and 10 mM GSH solution (DMSO/PBS = 5/2, v/v, pH = 7.4).

(TEM) analysis (Fig. 2A and Fig. S5, ESI†). In comparison to Cy-TK and LND, the maximum absorbance peak of synthetic Cy-TK-LND NPs was red-shifted by 10 nm and 20 nm in the UV-vis absorption spectrum due to π–π stacking, which might have increased the laser irradiation penetration depth (Fig. 2B). A similar effect could be observed in the fluorescence emission spectrum with an excitation wavelength of 650 nm (Fig. 2C).

The thioketal moiety can be readily cleaved when exposed to pathological levels of ROS;[44,45] thus we next evaluated the responsiveness of Cy-TK-LND NPs. The results of UV spectra indicated that a peak appeared at 800 nm when Cy-TK-LND NPs were exposed to H_2O_2 or GSH solution (Fig. 2D and Fig. S6, ESI†). Importantly, the absorbance of Cy-TK-LND NPs in the GSH solution at 800 nm increased over time, while it decreased at 650 nm. Furthermore, the absorption ratio (800 nm/650 nm) of Cy-TK-LND NPs was linearly related to GSH concentration (Fig. S7, ESI†). Fluorescence emission spectra displayed that the fluorescence intensity of Cy-TK-LND NPs exposed to increasing concentrations of H_2O_2 or GSH solution gradually decreased at 780 nm or 750 nm (Fig. S8, ESI†). Moreover, changes in the particle size distribution and an increased PDI index also indicated that the structure of Cy-TK-LND NPs was disrupted after being exposed to GSH (Fig. S9, ESI†). Similar results were shown when Cy-TK-LND NPs were exposed to 660 nm laser radiation; the reason may be that the endogenous ROS produced by the photosensitizer Cy after illumination promoted the breakage of the TK linker.

Thus, the ROS generation from Cy-TK-LND NPs was next assessed using non-fluorescence 2′,7′-dichlorodihydrofluorescein diacetate (DCFH-DA). This indicator could be rapidly oxidized into highly fluorescent 2′,7′-dichlorofluorescein (DCF) in the presence of ROS. The result showed that the fluorescence intensity of the emission peak at 525 nm gradually increased, indicating the enhanced ROS production from Cy-TK-LND NPs with laser irradiation (Fig. S10, ESI†). The above results demonstrate that laser radiation triggers the disintegration of Cy-TK-LND NPs in response to ROS/GSH.

It has been proven that the members of OATPs can mediate the transmembrane transport of compounds.[46] To confirm the interaction between the Cy-TK-LND NPs and OATPs, the OATP1B3 was selected as the receptor for molecular docking. The structure of OATP1B3 was obtained from the computed structure model (AlphaFold DB: AF_AFQ9NPD5F1). The result indicated that Cy-TK-LND NPs were embedded in the groove of the OATP1B3 protein with close contacts (Fig. S11, ESI†). The binding site residues included five residues with hydrophobic interactions (LEU148, PHE150, LYS125, ILE129, and VAL158) and two hydrogen bound residues (GLU165 and SER606). To further determine whether the uptake of Cy-TK-LND NPs is related to OATPs, 4T1 was pretreated with sulfobromophthalein (BSP), a competitive inhibitor of OATPs.[47,48] The flow cytometry and confocal results both showed that BSP significantly inhibited the uptake of Cy-TK-LND NPs by cancer cells (Fig. S12 and S13, ESI†). Moreover, compared to pravastatin (OATP1B1-specific inhibitor) and itraconazole (OATP2B1-specific inhibitor), selective inhibitors of OATP1B3 (vincristine) demonstrated notable impacts on the transport of Cy-TK-LND NPs. These results demonstrate the high uptake of Cy-TK-LND NPs by cancer cells without the conjugation of the target moiety.

A study reported that a lipophilic cation could accumulate in the highly negatively charged mitochondrial matrix microenvironment to a great extent.[37] Thus, the intracellular localization of Cy-TK-LND NPs was investigated by confocal laser scanning microscope (CLSM). HeLa cells were co-incubated with Cy-TK-LND NPs for 30 min and then stained with ER-Tracker, Lyso-Tracker, and Mito-Tracker. The CLSM images and Pearson's correlation coefficient showed that the Cy-TK-LND NPs were poorly co-localized with the endoplasmic reticulum (ER) and lysosomes (Fig. 3). In contrast, Cy-TK-LND NPs could be preferentially accumulated in the mitochondria. Analysis of the colocalization results demonstrates that Cy-TK-LND NPs possess the mitochondrial-targeting property, providing the possibility to achieve effective chemotherapy drug delivery and therapeutic efficacy.

The potential to target mitochondria may induce a high level of ROS production. To validate this hypothesis, intracellular ROS generation after different treatments was examined by using a DCFH-DA probe. The flow cytometry result showed that the relative level of ROS content in 4T1 cells treated with Cy-TK-LND NPs under laser irradiation was higher than that of other groups (Fig. S14, ESI†). One reason is that the Cy-TK-LND NPs maintained the photosensitive characteristic of Cy, enhancing the oxidative stress of the cancer cells with laser irradiation. Another reason is that the mitochondria-targeted delivery of chemotherapeutic agents disrupted the energy metabolism of cancer cells. Therefore, the mean fluorescence intensity of Cy-TK-LND NPs was more than three times stronger than that of LND even uder the dark condition. Significantly, the perturbation of redox homeostasis and induction of oxidative stress can further lead to cell apoptosis.

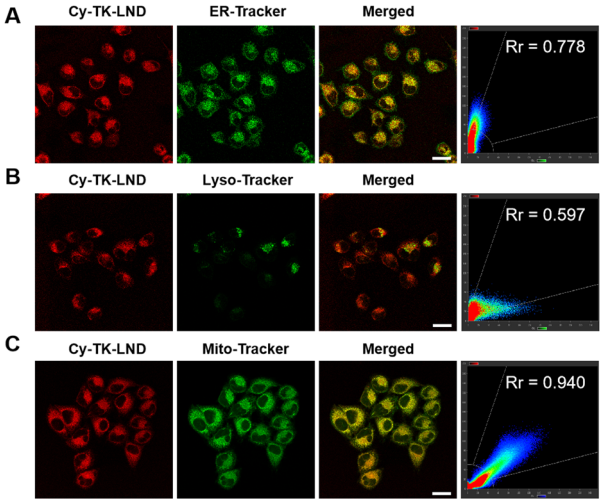

Fig. 3 Mitochondria-specific localization of Cy-TK-LND NPs. The CLSM images of HeLa cells after treatment with Cy-TK-LND NPs and staining with ER-Tracker (A), Lyso-Tracker (B), and Mito-Tracker (C) (scale bar, 25 μm).

Therefore, we next evaluated the *in vitro* cytotoxicity of Cy-TK-LND NPs, and cell counting kit-8 (CCK-8) assay was performed with the tumor cells (4T1 cells and A549 cells). The results showed that Cy-TK-LND NPs with laser irradiation displayed more significant cytotoxicity compared with the non-irradiated counterpart (Fig. 4 and Fig. S15, ESI†). The reason is that the ROS content in tumor cells is insufficient to completely trigger the breakage of the TK linker. To excellently exhibit anti-tumor activity, it is critical that the 660 nm laser irradiation-induced oxidative stress increases the level of ROS, leading to an on-demand release of free LND. Notably, the low concentration LND with or without light both showed a negligible cytotoxicity effect due to its poor solubility in the cytoplasm. Furthermore, the IC_{50} value of irradiated Cy-TK-LND NPs was 11.06 μM against 4T1 cells, which was 5-fold lower than that of LND and 2-fold lower than that of Cy. These results state that Cy-TK-LND NPs significantly enhanced the antitumor effect of LND.

The mechanism by which Cy-TK-LND NPs led to cell death was further investigated. The study confirmed that LND could cause apoptosis by directly impacting the mitochondria.[49] Mitochondrial depolarization is considered an early event during the apoptosis cascade.[50] Therefore, the mitochondrial membrane potential was first evaluated using JC-1 staining assay. Green fluorescent JC-1 monomers could enter the cells

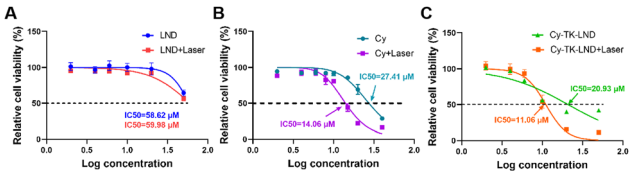

Fig. 4 The IC_{50} value of 4T1 cells incubated with LND, Cy, and Cy-TK-LND NPs, and light groups were exposed to laser for 20 min.

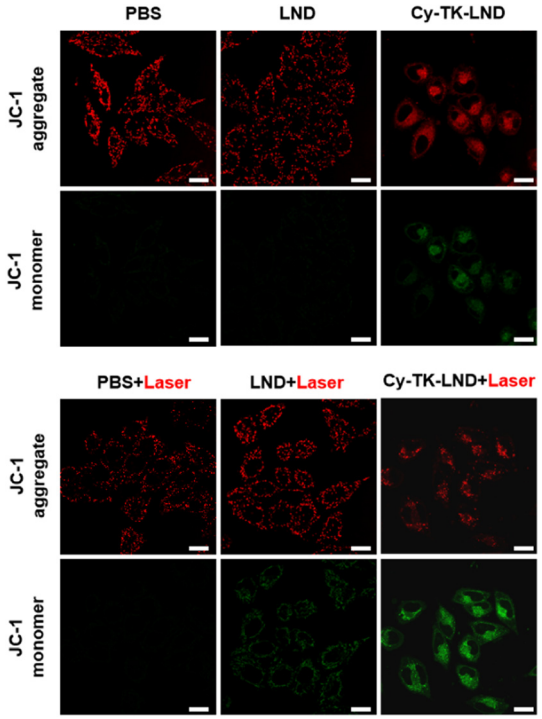

Fig. 5 Cy-TK-LND NPs induced mitochondrial membrane potential decline. The CLSM images of 4T1 cells were stained with JC-1 after different materials without or with laser irradiation (scale bar, 20 μm).

and aggregate in the matrix of normal mitochondria, forming a polymer (JC-1 aggregate) with red fluorescence. Thus, the fluorescence signal change from red to green indicates that the membrane potential declined and mitochondrial dysfunction began. The result indicated that the PBS, LND, and only laser groups displayed a nonsignificant fluorescence change (Fig. 5). In contrast, increased green fluorescence while decreased red fluorescence was observed in 4T1 cells incubated with Cy-TK-LND NPs. More importantly, this transformation was more pronounced in the Cy-TK-LND plus laser irradiation group, and the morphology of mitochondria gradually punctated, indicating severe mitochondrial damage in cancer cells. Interestingly, the LND + laser group displayed a slight green fluorescence. This finding suggests that the pharmacological effect of LND is diminished due to lack of its mitochondrial targeting ability.

Moreover, mitochondrial disorder causes a decrease in the production of adenosine triphosphate (ATP). We next examined the level of cellular ATP using an ATP assay kit. The result showed that the extracellular ATP level was moderately increased after laser irradiation in the LND group, but no statistically significant difference ($p > 0.05$) was observed (Fig. S16, ESI†). The reason is probably that the light weakly enhanced the occurrence of LND-induced immunogenic cell death (ICD), leading to the active secretion of ATP from cells to express the "eat me" signal.[51] Oppositely, under 660 nm laser irradiation, the ATP content significantly decreased in the cells incubated with Cy-TK-LND NPs, and the relative ATP concentration was 4 times lower compared with that in the control

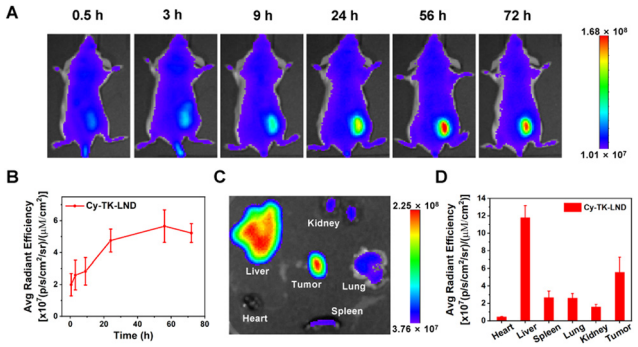

Fig. 6 The biodistribution of Cy-TK-LND NPs *in vivo*. (A) Time-lapse fluorescence images of the mice after intravenous administration of Cy-TK-LND NPs (50 μM, 100 μL). (B) Fluorescence intensity of tumor in the mice at different time points after administration of Cy-TK-LND NPs (n = 3). (C) Fluorescence images of major organs and tumors of the mice 72 h post-injection. (D) Statistical analysis of fluorescence intensity in (C) (n = 3).

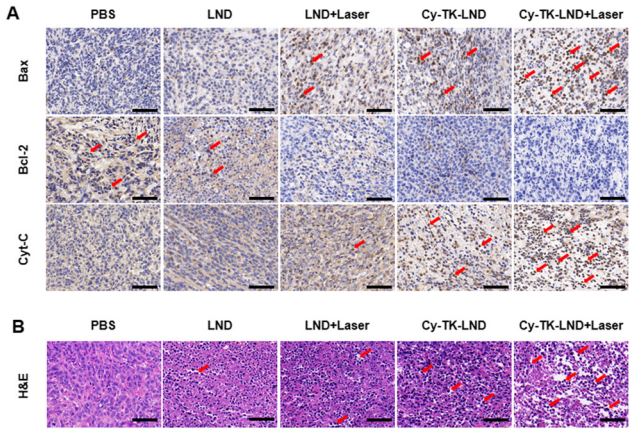

Fig. 8 Immunohistochemistry (A) and H&E staining (B) of tumor sections in the mice after tail vein injection with LND or Cy-TK-LND NPs; the light groups were irradiated with a 660 nm laser for 20 min after 48 h of injection (scale bar, 50 μm). The red arrows in (A) and (B) point to the corresponding protein upregulation and cell death, respectively.

group. In this case, the Cy-TK-LND NPs damage to the mitochondria accounts for a major role. The reduction in ATP levels demonstrates that the effective release of LND inhibited the hexokinase activity, glycolytic pathway, and the metabolism of cancer cells.

To explore the *in vivo* biodistribution of Cy-TK-LND NPs, 100 μL of Cy-TK-LND NPs (50 μM in the solution of PBS) was intravenously injected into the 4T1 tumor-bearing mice. *In vivo* fluorescence imaging displayed that the fluorescent signal was initially noticed at the tumor site of mice at 0.5 h after administration (Fig. 6A). After 56 h of injection, the prominent tumor fluorescence enrichment phenomenon was displayed to reach a maximum, still maintaining an apparent signal at 72 h (Fig. 6B and Fig. S17, ESI†). Importantly, the fluorescence intensity at the tumor site was the highest in addition to liver accumulation (Fig. 6C and D). These phenomena demonstrate that Cy-TK-LND NPs possess excellent tumor targeting *in vivo*, and are mainly cleared by liver metabolism.

To further validate the antitumor effect of Cy-TK-LND NPs *in vivo*, we injected various drugs into tumor-bearing mice. After 48 h, the tumor area was irradiated for 10 min. The results showed that the irradiated Cy-TK-LND NPs significantly inhibited tumor growth (Fig. 7). In addition, no abnormal changes in body weight were observed in the treated mice. Then, tumor site sections derived from mice after different treatments were used for immunohistochemical analysis and hematoxylin and eosin (H&E) staining (Fig. 8). Compared to other groups, the expression level of pro-apoptotic Bax and cytochrome *C* were upregulated, while anti-apoptotic Bcl-2 was downregulated in the Cy-TK-LND NPs plus laser irradiation group. Moreover, significant apoptotic and necrotic cells were observed in the tumor tissues of mice treated with Cy-TK-LND NPs under laser irradiation, implicating its marked effect on cancer treatment. These phenomena illustrate the induction of the mitochondria-mediated apoptotic pathway.

Based on the superior therapeutic efficacy, the biosafety of Cy-TK-LND NPs *in vivo* was further evaluated. H&E staining of major organs displayed no noticeable differences between any groups, indicating reduced adverse side effects (Fig. S18, ESI†). Furthermore, the hematological data and liver and kidney function index were investigated to further demonstrate the biosafety of Cy-TK-LND NPs (Fig. 9 and Fig. S19, ESI†).

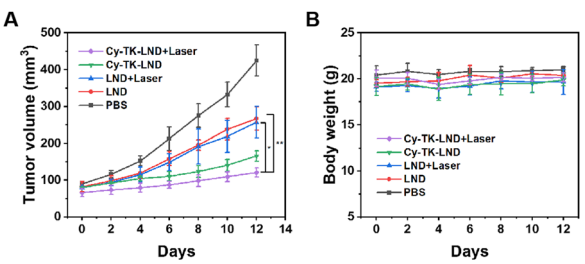

Fig. 7 Antitumor effect of Cy-TK-LND NPs *in vivo*. (A) Tumor growth curves of the treated mice. (B) Body weight of the mice after the various treatments. *P < 0.05 and **P < 0.01.

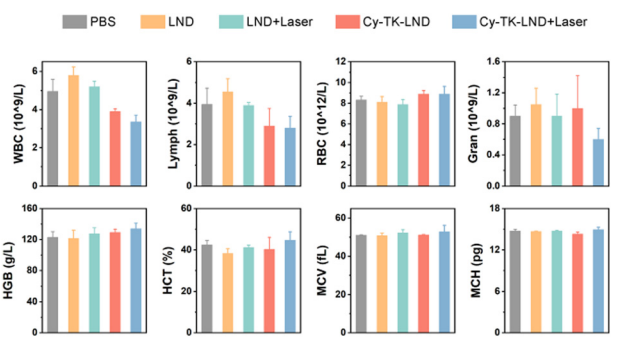

Fig. 9 Hematological data of samples from the mice after different treatments. The terms are noted as follows: white blood cells (WBCs), lymphocyte (lymph), red blood cells (RBCs), neutrophilic granulocyte (Gran), hemoglobin (HGB), hematocrit (HCT), mean corpuscular volume (MCV), and mean corpuscular hemoglobin (MCH).

Conclusions

In general, we successfully engineered redox-activated self-assembled carrier-free nanoparticles (Cy-TK-LND NPs) based on a prodrug for cancer precision chemotherapy. The targeted lipophilic cation IR780 could precisely deliver the Cy-TK-LND NPs to the mitochondria of cancer cells. Oxidative stress within tumor cells was enhanced by controlling the external light irradiation, causing the spatiotemporal release of free LND to ensure tumor-targeted therapeutic activity. Interestingly, the elevated level of ROS by the action of LND on mitochondria in turn promoted the drug release, thus allowing for self-circulation. *In vitro* and *in vivo* assays demonstrated the obvious toxic effect of Cy-TK-LND NPs plus laser irradiation on cancer cells. The relevant mechanism is the activation of the mitochondria-mediated apoptotic pathway, which is characterized by a decrease in membrane potential, reduced ATP synthesis, and release of cytochrome *C* into the cytoplasm. The expression changes of the apoptosis-related proteins indicate the activation of the mitochondrial apoptosis pathway caused by the Cy-TK-LND NPs. Overall, this work demonstrates that using targeted Cy-TK-LND NPs is a promising strategy for enhanced cancer chemotherapy by disrupting mitochondrial metabolism.

Author contributions

Ting Yang: conceptualization, formal analysis, methodology, software, visualization, and writing – original draft. Xianfen Zhang: data curation, formal analysis, methodology, investigation, visualization, and software. Xing Yang: conceptualization, methodology, and visualization. Ying Li: methodology, investigation. Jingjing Xiang: formal analysis, and software. Chunbai Xiang: formal analysis and validation. Zhongke Liu: validation. Luo Hai: validation. Saipeng Huang: supervision, resources, and methodology. Lihua Zhou: conceptualization, funding acquisition, project administration, and writing – review and editing. Ruijing Liang: conceptualization, resources, supervision, and visualization. Ping Gong: funding acquisition, project administration, supervision, and writing – review and editing.

Conflicts of interest

There are no conflicts to declare.

Acknowledgements

This work was partially supported by the National Key R&D Programs (2021YFA0910001), the Shenzhen Science and Technology Program (JCYJ20210324115804013, JCYJ2022081810160716, and JCYJ20200109114616534), the Shenzhen-Macao Technology Plan (SGDX2020110309280301), the National Natural Science Foundation of China (22005343), the Guangdong Provincial Key Area R&D Program (2020B1111540001), and the Research Program of Shenzhen Institute of Technology (2111015). We thank for the help from the office of Research and Development of Shenzhen Institute of Technology (SIT).

Notes and references

1 W. Fan, B. Yung, P. Huang and X. Chen, *Chem. Rev.*, 2017, **117**, 13566–13638.
2 R. Duncan, *Nat. Rev. Cancer*, 2006, **6**, 688–701.
3 C. Y. Zhao, R. Cheng, Z. Yang and Z. M. Tian, *Molecules*, 2018, **23**, 826.
4 L. Zhou, H. Wang and Y. Li, *Theranostics*, 2018, **8**, 1059–1074.
5 D. J. Bharali and S. A. Mousa, *Pharmacol. Ther.*, 2010, **128**, 324–335.
6 B. Feng, Z. Niu, B. Hou, L. Zhou, Y. Li and H. Yu, *Adv. Funct. Mater.*, 2019, **30**, 1906605.
7 S. Tran, P. J. DeGiovanni, B. Piel and P. Rai, *Clin. Transl. Med.*, 2017, **6**, 44.
8 X. Xu, W. Ho, X. Zhang, N. Bertrand and O. Farokhzad, *Trends Mol. Med.*, 2015, **21**, 223–232.
9 H. Chen, Z. Gu, H. An, C. Chen, J. Chen, R. Cui, S. Chen, W. Chen, X. Chen, X. Chen, Z. Chen, B. Ding, Q. Dong, Q. Fan, T. Fu, D. Hou, Q. Jiang, H. Ke, X. Jiang, G. Liu, S. Li, T. Li, Z. Liu, G. Nie, M. Ovais, D. Pang, N. Qiu, Y. Shen, H. Tian, C. Wang, H. Wang, Z. Wang, H. Xu, J.-F. Xu, X. Yang, S. Zhu, X. Zheng, X. Zhang, Y. Zhao, W. Tan, X. Zhang and Y. Zhao, *Sci. China: Chem.*, 2018, **61**, 1503–1552.
10 Q. Yin, J. Shen, Z. Zhang, H. Yu and Y. Li, *Adv. Drug Delivery Rev.*, 2013, **65**, 1699–1715.
11 X. Du, L. Xiong, S. Dai and S. Z. Qiao, *Adv. Healthcare Mater.*, 2015, **4**, 771–781.
12 S. Bamrungsap, Z. L. Zhao, T. Chen, L. Wang, C. M. Li, T. Fu and W. H. Tan, *Nanomedicine*, 2012, **7**, 1253–1271.
13 R. Ni, J. Zhu, Z. Xu and Y. Chen, *J. Mater. Chem. B*, 2020, **8**, 1290–1301.
14 D. Zhao, W. Tao, S. Li, L. Li, Y. Sun, G. Li, G. Wang, Y. Wang, B. Lin, C. Luo, Y. Wang, M. Cheng, Z. He and J. Sun, *Nanoscale Horiz.*, 2020, **5**, 886–894.
15 L. Xi, J. Wang, Y. Wang and Z. Ge, *Macromol. Biosci.*, 2021, **21**, e2100091.
16 T. Qi, B. Chen, Z. Wang, H. Du, D. Liu, Q. Yin, B. Liu, Q. Zhang and Y. Wang, *Biomaterials*, 2019, **213**, 119219.
17 M. Karimi, P. Sahandi Zangabad, S. Baghaee-Ravari, M. Ghazadeh, H. Mirshekari and M. R. Hamblin, *J. Am. Chem. Soc.*, 2017, **139**, 4584–4610.
18 M. Liu, A. R. Khan, J. Ji, G. Lin, X. Zhao and G. Zhai, *J. Controlled Release*, 2018, **290**, 150–164.
19 Y. Tian, X. Jiang, X. Chen, Z. Shao and W. Yang, *Adv. Mater.*, 2014, **26**, 7393–7398.
20 D. Li, R. Zhang, G. Liu, Y. Kang and J. Wu, *Adv. Healthcare Mater.*, 2020, **9**, e2000605.
21 X. Guo, Y. Cheng, X. Zhao, Y. Luo, J. Chen and W. E. Yuan, *J. Nanobiotechnol.*, 2018, **16**, 74.

22 R. Li, F. Peng, J. Cai, D. Yang and P. Zhang, *Asian J. Pharm. Sci*, 2020, **15**, 311–325.
23 D. Chen, G. Zhang, R. Li, M. Guan, X. Wang, T. Zou, Y. Zhang, C. Wang, C. Shu, H. Hong and L. J. Wan, *J. Am. Chem. Soc.*, 2018, **140**, 7373–7376.
24 B. Sun, C. Luo, H. Yu, X. Zhang, Q. Chen, W. Yang, M. Wang, Q. Kan, H. Zhang, Y. Wang, Z. He and J. Sun, *Nano Lett.*, 2018, **18**, 3643–3650.
25 C. Xu, H. Yang, Z. Xiao, T. Zhang, Z. Guan, J. Chen, H. Lai, X. Xu, Y. Huang, Z. Huang and C. Zhao, *Int. J. Pharm.*, 2021, **603**, 120671.
26 M. Y. Yang, R. R. Zhao, Y. F. Fang, J. L. Jiang, X. T. Yuan and J. W. Shao, *Int. J. Pharm.*, 2019, **570**, 118663.
27 Y. Li, J. Lin, Z. Cai, P. Wang, Q. Luo, C. Yao, Y. Zhang, Z. Hou, J. Liu and X. Liu, *J. Controlled Release*, 2020, **321**, 222–235.
28 C. Yu, M. Zhou, X. Zhang, W. Wei, X. Chen and X. Zhang, *Nanoscale*, 2015, **7**, 5683–5690.
29 X. Zhao, H. Zhao, S. Wang, Z. Fan, Y. Ma, Y. Yin, W. Wang, R. Xi and M. Meng, *J. Am. Chem. Soc.*, 2021, **143**, 20828–20836.
30 C. Zhang, L. Long and C. Shi, *Adv. Ther.*, 2018, **1**, 1800069.
31 E. Zhang, S. Luo, X. Tan and C. Shi, *Biomaterials*, 2014, **35**, 771–778.
32 S. Luo, X. Tan, S. Fang, Y. Wang, T. Liu, X. Wang, Y. Yuan, H. Sun, Q. Qi and C. Shi, *Adv. Funct. Mater.*, 2016, **26**, 2826–2835.
33 X. Tan, S. Luo, L. Long, Y. Wang, D. Wang, S. Fang, Q. Ouyang, Y. Su, T. Cheng and C. Shi, *Adv. Mater.*, 2017, **29**, 1704196.
34 Q. Chen, N. Li, X. Wang, Y. Yang, Y. Xiang, X. Long, J. Zhang, J. Huang, L. Chen and Q. Huang, *Front. Pharmacol.*, 2022, **13**, 847048.
35 L. Jiang, S. S. Zhou, X. K. Zhang, C. Li, S. L. Ji, H. Mao and X. Q. Jiang, *Nat. Commun.*, 2021, **12**, 2390.
36 C. Dong, Z. Liu, J. Liu, C. Wu, F. Neumann, H. Wang, M. Schafer-Korting, B. Kleuser, J. Chang, W. Li, N. Ma and R. Haag, *Adv. Healthcare Mater.*, 2016, **5**, 2214–2226.
37 G. Battogtokh, Y. S. Choi, D. S. Kang, S. J. Park, M. S. Shim, K. M. Huh, Y. Y. Cho, J. Y. Lee, H. S. Lee and H. C. Kang, *Acta Pharm. Sin. B*, 2018, **8**, 862–880.
38 L. Ren, P. Xu, J. Yao, Z. Wang, K. Shi, W. Han and H. Wang, *ACS Nano*, 2022, **16**, 10242–10259.
39 Y. Han, C. Gao, H. Wang, J. Sun, M. Liang, Y. Feng, Q. Liu, S. Fu, L. Cui, C. Gao, Y. Li, Y. Yang and B. Sun, *Bioact. Mater.*, 2021, **6**, 529–542.
40 G. Cheng, Q. Zhang, J. Pan, Y. Lee, O. Ouari, M. Hardy, M. Zielonka, C. R. Myers, J. Zielonka, K. Weh, A. C. Chang, G. Chen, L. Kresty, B. Kalyanaraman and M. You, *Nat. Commun.*, 2019, **10**, 2205.
41 Y. Liu, X. Zhang, M. Zhou, X. Nan, X. Chen and X. Zhang, *ACS Appl. Mater. Interfaces*, 2017, **9**, 43498–43507.
42 Y. Huang, G. Sun, X. Sun, F. Li, L. Zhao, R. Zhong and Y. Peng, *Cancers*, 2020, **12**, 3332.
43 M. Sun, C. Wang, M. Lv, Z. Fan and J. Du, *Biomaterials*, 2021, **278**, 121168.
44 A. Rinaldi, R. Caraffi, M. V. Grazioli, N. Oddone, L. Giardino, G. Tosi, M. A. Vandelli, L. Calza, B. Ruozi and J. T. Duskey, *Polymers*, 2022, **14**, 687.
45 X. Xia, X. Yang, P. Huang and D. Yan, *ACS Appl. Mater. Interfaces*, 2020, **12**, 18301–18308.
46 R. B. Kim, *Eur. J. Clin. Invest.*, 2003, **33**, 1–5.
47 A. Kalliokoski and M. Niemi, *Br. J. Pharmacol.*, 2009, **158**, 693–705.
48 X. Yang, C. Shi, R. Tong, W. Qian, H. E. Zhau, R. Wang, G. Zhu, J. Cheng, V. W. Yang, T. Cheng, M. Henary, L. Strekowski and L. W. K. Chung, *Clin. Cancer Res.*, 2010, **16**, 2833–2844.
49 N. Li, C. X. Zhang, X. X. Wang, L. Zhang, X. Ma, J. Zhou, R. J. Ju, X. Y. Li, W. Y. Zhao and W. L. Lu, *Biomaterials*, 2013, **34**, 3366–3380.
50 J. Lu, L. Wu, X. Wang, J. Zhu, J. Du and B. Shen, *J. Visualized Exp.*, 2018, **137**, e56317.
51 O. Krysko, T. Løve Aaes, C. Bachert, P. Vandenabeele and D. V. Krysko, *Cell Death Dis.*, 2013, **4**, e631.